Nanoparticle detection based on microcavity exceptional-point characteristics

Li-Li Zheng,[1] Xue-Hui Xiong,[1] Xin-Yue Guo,[2] Deng-Wei Zhang,[3,*] and Xin-You Lü[2]

[1]*Key Laboratory of Optoelectronic Chemical Materials and Devices of Ministry of Education, Jianghan University, Wuhan 430074, People's Republic of China*

[2]*School of Physics, Huazhong University of Science and Technology, Wuhan 430074, People's Republic of China*

[3]*Department of Mathematics and Physics, Luoyang Institute of Science and Technology, Luoyang 471023, People's Republic of China*

(Received 16 September 2023; accepted 8 December 2023; published 2 January 2024)

We investigate theoretically optomechanically induced transparency in a whispering-gallery-mode microresonator coupled with three nanoparticles. We find that the presence of the third nanoparticle makes the transmission rate more sensitive in the vicinities of exceptional points (EPs). In addition, we also find that adjusting the relative position of the nanoparticles so that the system is near or far from the EPs can realize the switching of the probe light between slow and fast light. Our finding not only provides an alternative way to tune the spread of light but also can identify the existence of the third particle by detecting the change in the output spectrum of light so as to achieve particle detection. Our work may have potential application value in optical signal processing and communication.

DOI: 10.1103/PhysRevA.109.013502

I. INTRODUCTION

Cavity optomechanics is a frontier field that studies the interaction between the optical field and mechanical oscillator [1]. Due to the optomechanical nonlinearity, the cavity optomechanical system provides an ideal platform for exploring many interesting quantum [2–12] and classical [13–27] phenomena. With the advancement of micro- and nanotechnology, the optical microcavity quality factor has consistently improved, and the mode sizes have been reduced, propelling the rapid development and applications of cavity optomechanics [28–36]. Optomechanically induced transparency (OMIT), a prominent phenomenon in cavity optomechanics, arises from the destructive interference between the Stokes field and the anti-Stokes field, which opens up novel avenues for coherent light control and even quantum memory applications [37–39]. Hence it has sparked widespread interest and has been thoroughly studied, such as exploring higher-order sidebands in OMIT [40,41], investigating its intriguing manifestations in hybridized optomechanical systems [42–51], and investigating nonreciprocal OMIT [52,53].

In recent years, properties and applications of exceptional points (EPs) have attracted much attention and shown great potential in optomechanical systems [54–61]. The physical mechanism of EPs leads to many novel and counterintuitive physical effects, such as the single-mode laser [62,63], the parity-time-symmetric ($\mathcal{PT}$-symmetric) phonon laser [64], $\mathcal{PT}$-symmetry-breaking chaos [65], sensitivity enhancement [66–69], and nonreciprocal optical transmission [70]. In particular, a phenomenon of EPs emerging periodically has been experimentally observed by coupling a whispering-gallery-mode (WGM) microresonator with two external nanoparticles and tuning their relative position of nanoparticles [71]. Recently, relevance theory also suggests that tuning the relative position of nanoparticles not only can achieve switching between slow and fast light but also can significantly change the OMIT spectrum in the vicinities of EPs [72]. Natural questions, when we consider the mode of a WGM microresonator coupling with three nanoparticles, are whether the transmission spectrum is affected by the presence of the third nanoparticle and whether this effect can be used to detect said nanoparticle. These questions remain unexplored in cavity optomechanics, which may have potential application value in optical signal processing and communication.

In this paper, we theoretically investigate OMIT in an optomechanical system consisting of a WGM microresonator coupled with three nanoparticles. Physically, the presence of nanoparticles causes the asymmetrical backscattering of resonator modes, leading to significant changes in the optical properties in the vicinities of EPs [66,67]. Therefore we propose utilizing the phenomenon of OMIT in the vicinities of EPs to detect the third nanoparticle by tuning the relative position of the nanoparticles. To date, although a number of studies have investigated the impact EPs have on OMIT, there are few theories to explore the influence of the third nanoparticle on the phenomenon. The study of the phenomenon is valuable for optical signal processing and communications. In order to clearly show the impact of the third particle on OMIT and group delay, we derive the expressions of the transmittance rate and discuss in detail the influence of the third nanoparticle on the phenomenon. On these bases, our findings demonstrate that the third nanoparticle increases OMIT sensitivity and results in the emergence of the slow-light effect in the vicinities of EPs, which not only offers a means to control light propagation but also provides a method to detect the existence of the third nanoparticle by utilizing the change in the output spectrum. Our work may offer an alternative avenue

*zdw161@126.com

 ©2024 American Physical Society

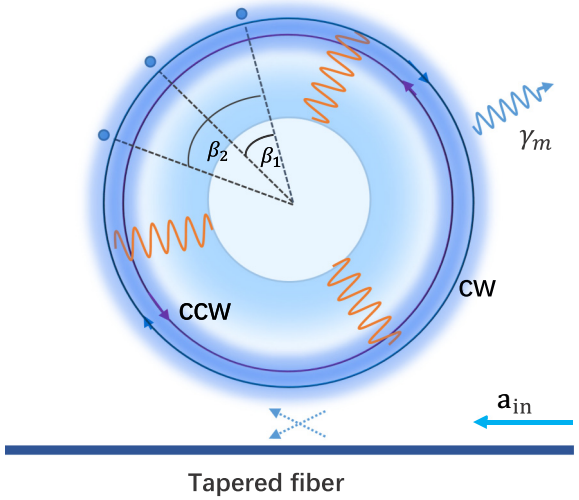

FIG. 1. Schematic of the optomechanical system consisting of a tapered fiber and a WGM microresonator coupled with three nanoparticles. The microresonator also supports a mechanical mode with frequency ω_m and damping rate γ_m. The system is driven by a pump field with frequency ω_l and a probe field with frequency ω_p. β_1 and β_2 represent the relative angles between the three particles.

for improving precision measurement and its application in optically sensitive detection.

This work is organized as follows: In Sec. II, we provide a detailed introduction to the system model and Hamiltonian. We then identify the EPs by solving the system's eigenvalues and reveal the periodic occurrence pattern of these points. Furthermore, we present the OMIT solution by calculating the Heisenberg-Langevin equations and utilizing the input-output relation. In Sec. III, based on the analytical calculations, we discuss the phenomenon of OMIT and exploit the sensitive characteristic in the vicinities of EPs to realize nanoparticle detection. In Sec. IV, we finally summarize our work.

II. MODEL

We consider a WGM microresonator coupled to a fiber-taper waveguide, which supports clockwise-traveling (CW traveling) and counterclockwise-traveling (CCW traveling) modes and contains a mechanical breathing mode, as shown in Fig. 1. In the resonator, three nanoparticles as Rayleigh scatterers are introduced in the evanescent field to tune the coupling between CW and CCW modes to impact the system property. The optical coupling strengths between the CW and CCW modes caused by the nanoparticles can be expressed as [68]

$$J_1 = \epsilon_1 + \epsilon_2 e^{-i2m\beta_1} + \epsilon_3 e^{-i2m\beta_2},$$
$$J_2 = \epsilon_1 + \epsilon_2 e^{i2m\beta_1} + \epsilon_3 e^{i2m\beta_2}, \tag{1}$$

where J_1 (J_2) quantifies the strength of the reflection of light from the CW (CCW) mode to the CCW (CW) mode. Here, ϵ_j ($j = 1, 2, 3$) denotes half of the complex frequency splitting caused by the jth nanoparticle, m is the azimuthal mode number, and the phase angles β_1 and β_2 represent the relative positions of nanoparticles, as shown in Fig. 1. These nanoparticles can be fabricated by heating and stretching standard optical fibers, and the relative phase angles β_1 and β_2 can be controlled by nanopositioners. The resonator (with resonance frequency ω_a) is driven by a strong pump field with frequency ω_l and a weak probe field with frequency ω_p. In a rotating frame with the pump frequency ω_l, the total Hamiltonian of the system can be written as

$$\hat{H} = \hat{H}_0 + \hat{H}_{\rm int} + \hat{H}_{\rm dr}, \tag{2}$$

with

$$\begin{aligned}\hat{H}_0 &= \frac{\hat{p}^2}{2m_{\rm eff}} + \frac{1}{2}m_{\rm eff}\omega_m^2\hat{x}^2 + \hbar\Delta\hat{a}_{\rm cw}^\dagger\hat{a}_{\rm cw} + \hbar\Delta\hat{a}_{\rm ccw}^\dagger\hat{a}_{\rm ccw},\\ \hat{H}_{\rm int} &= -\hbar g\hat{x}(\hat{a}_{\rm cw}^\dagger\hat{a}_{\rm cw} + \hat{a}_{\rm ccw}^\dagger\hat{a}_{\rm ccw}) + \hbar J_1\hat{a}_{\rm cw}^\dagger\hat{a}_{\rm ccw}\\ &\quad + \hbar J_2\hat{a}_{\rm ccw}^\dagger\hat{a}_{\rm cw},\\ \hat{H}_{\rm dr} &= i\hbar\sqrt{\eta\gamma_a}[(E_l + E_p e^{-i\xi t})\hat{a}_{\rm cw}^\dagger - \text{H.c.}],\end{aligned} \tag{3}$$

where $\hat{x}$ ($\hat{p}$) is the dimensionless displacement (momentum) operator of the mechanical breathing mode with the effective mass $m_{\rm eff}$ and frequency ω_m. $\hat{a}_{\rm cw}$ ($\hat{a}_{\rm cw}^\dagger$) and $\hat{a}_{\rm ccw}$ ($\hat{a}_{\rm ccw}^\dagger$) are the annihilation (creation) operators of the CW and CCW modes, respectively, with the same resonance frequency ω_a and damping γ_a. The detuning between the cavity field and the pump laser $\Delta = \omega_a - \omega_l + \text{Re}(\epsilon_1 + \epsilon_2 + \epsilon_3)$, where $\text{Re}(\epsilon_1 + \epsilon_2 + \epsilon_3)$ is the perturbation frequency of the cavity mode induced by nanoparticles [71,73]. The Hamiltonian $\hat{H}_{\rm int}$ represents the interaction between the CW field, the CCW field, and mechanical deformation, which affect each other through the optical coupling strength and optomechanical interaction. The coupling strength between the cavity modes and the mechanical oscillator is represented by $g = \omega_a/R$, where R denotes the radius of the resonator [29]. The resonator is driven by a pump laser with frequency ω_l and amplitude $E_l = \sqrt{P_l/\hbar\omega_l}$, and a probe laser with frequency ω_p and amplitude $E_p = \sqrt{P_p/\hbar\omega_p}$, where P_l and P_p are the driving power of the pump and probe light, respectively. γ_a is the loss rate consisting of an external loss rate $\gamma_{\rm ex}$ induced by the resonator-fiber coupling and an intrinsic loss rate γ_0. The parameter $\eta = \gamma_{\rm ex}/\gamma_a$, which can be continuously adjusted [38]. The detuning between the probe field and the pump field is given by $\xi = \omega_p - \omega_l$.

The presence of the nanoparticles results in frequency splitting of the optical modes, with the corresponding eigenfrequencies

$$\omega_{1,2} = \Delta - i\frac{\gamma_a}{2} + \sum_{j=1}^{3}\epsilon_j \pm \sqrt{J_1 J_2}, \tag{4}$$

where $+$ $(-)$ corresponds to ω_1 (ω_2). $J_1J_2 = \sum_{j=1}^3\epsilon_j^2 + 2\epsilon_1\epsilon_2\cos(2m\beta_1) + 2\epsilon_1\epsilon_3\cos(2m\beta_2) + 2\epsilon_2\epsilon_3\cos[2m(\beta_1-\beta_2)]$. The frequency splitting is defined as $\Delta\omega = \omega_1 - \omega_2$. Equation (4) clearly shows that $\Delta\omega$ is dependent on β_1 and β_2. Therefore one can steer the angles β_1 and β_2 to bring the system to an EP. In Fig. 2, we present the variation of $\Delta\omega$ as a function of β_2 when β_1 is fixed. Figure 2 clearly illustrates the periodic oscillations of the frequency splitting $\Delta\omega$ with changes in the angle β_2, which are evident due to the complex property of $\epsilon_{j=1,2,3}$. Importantly, Fig. 2 also reveals that adjusting the angles can push the system close to the EPs. Interestingly, the system exhibits two sets of EPs. One set is as follows: When tuning $\beta_1 \approx 0.215, 1.01, 1.79\ldots$,

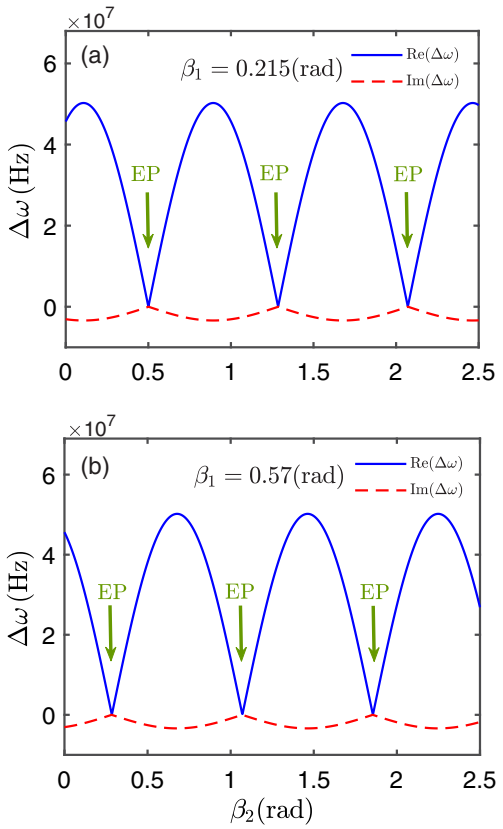

FIG. 2. (a) and (b) Diagrams of the complex frequency splitting $\Delta\omega$ induced by the relative angles of the nanoparticles β_1 and β_2, where the blue solid curves and pink dashed curves represent the real and imaginary parts of the complex frequency splitting of optical modes, respectively. The experimentally feasible values are $\omega_a = 193$ THz, $\omega_m = 125$ MHz, $\gamma_a = 2\gamma_{\rm ex} = 12.86$ THz, $\gamma_m = 3.82 \times 10^4$ Hz, $\epsilon_1/\gamma_{\rm ex} = 1.5 - 0.1i$, $\epsilon_2/\gamma_{\rm ex} = 1.4999 - 0.101\,489i$, $\epsilon_2/\gamma_{\rm ex} = 1.9499 - 0.1319i$, $R = 34.5$ μm, $g = \omega_a/R$, $m_{\rm eff} = 50$ ng, and the azimuthal mode number $m = 4$ [71,72].

EPs emerge around $\beta_2 \approx 0.5, 1.28, 2.07\ldots$. The other set is as follows: With the values $\beta_1 \approx 0.57, 1.355, 2.14\ldots$, EPs periodically emerge around $\beta_2 \approx 0.28, 1.07, 1.85\ldots$. Here, we only present the cases of $\beta_1 \approx 0.215$ and $\beta_1 \approx 0.57$, as shown in Figs. 2(a) and 2(b). The figure clearly elucidates the role of the relative angles β_1 and β_2 in EPs. Therefore the relative positions of nanoparticles have an important effect on the absorption of probe light. In the following, our primary goal is to investigate the influence of the third nanoparticle on OMIT in the vicinities of EPs.

Since we focus on the mean response of the system, any operator $\hat{o}$ can be simplified to a numerical value o, which allows us to describe the dynamical property of the system by using the semiclassical Langevin equations

$$\begin{aligned}
\dot{a}_{\rm cw} &= -(i\Delta - igx + \gamma)a_{\rm cw} - iJ_1 a_{\rm ccw} + \sqrt{\gamma_{\rm ex}}E_l \\
&\quad + \sqrt{\gamma_{\rm ex}}E_p e^{-i\xi t}, \\
\dot{a}_{\rm ccw} &= -(i\Delta - igx + \gamma)a_{\rm ccw} - iJ_2 a_{\rm cw}, \\
\ddot{x} &= -\gamma_m \dot{x} - \omega_m^2 x + \frac{\hbar g}{m_{\rm eff}}(a_{\rm cw}^\dagger a_{\rm cw} + a_{\rm ccw}^\dagger a_{\rm ccw}).
\end{aligned} \tag{5}$$

Here, we have safely ignored the photon-phonon quantum correlations in the semiclassical approximation. The parameter $\gamma = \gamma_a/2 - {\rm Im}(\epsilon_1 + \epsilon_2 + \epsilon_3)$ represents the total decay rate of the cavity mode, where ${\rm Im}(\epsilon_1 + \epsilon_2 + \epsilon_3)$ is the perturbation loss of the cavity mode induced by nanoparticles. From Eqs. (5), we can obtain the steady-state values

$$\begin{aligned}
\bar{a}_{\rm cw} &= \frac{\sqrt{\gamma_{\rm ex}}E_l(i\Delta - ig\bar{x} + \gamma)}{(i\Delta - ig\bar{x} + \gamma)^2 + J_1 J_2}, \\
\bar{a}_{\rm ccw} &= \frac{-\sqrt{\gamma_{\rm ex}}E_l J_2}{(i\Delta - ig\bar{x} + \gamma)^2 + J_1 J_2}, \\
\bar{x} &= \frac{\hbar g \gamma_{\rm ex}|E_l|^2[|J_2|^2 + \gamma^2 + (i\Delta - g\bar{x})^2]}{m_{\rm eff}\omega_{\rm m}^2|(i\Delta - ig\bar{x} + \gamma)^2 + J_1 J_2|^2}.
\end{aligned} \tag{6}$$

Since the intensity of the pump field is far greater than that of the probe field, i.e., $E_p \ll E_l$, one can regard the probe field as a perturbation to study the impact on the OMIT. Expanding each variable o as the sum of its steady-state and perturbation values, i.e., $o = \bar{o} + \delta o$, and substituting the ansatz into Eqs. (6), the perturbed dynamical equations read as follows:

$$\begin{aligned}
\dot{\delta a}_{\rm cw} &= -\Theta\delta a_{\rm cw} - ig\bar{a}_{\rm cw}\delta_x - iJ_1\delta a_{\rm ccw} + \sqrt{\gamma_{\rm ex}}E_p e^{-i\xi t}, \\
\dot{\delta a}_{\rm ccw} &= -\Theta\delta a_{\rm ccw} - ig\bar{a}_{\rm ccw}\delta_x - iJ_2\delta a_{\rm cw}, \\
\Phi\delta x &= \frac{\hbar g}{m_{\rm eff}}(\bar{a}_{\rm cw}\delta a_{\rm cw}^* + \bar{a}_{\rm cw}^*\delta a_{\rm cw} + \bar{a}_{\rm ccw}\delta a_{\rm ccw}^*) \\
&\quad + \frac{\hbar g}{m_{\rm eff}}\bar{a}_{\rm ccw}^*\delta a_{\rm ccw},
\end{aligned} \tag{7}$$

where $\Theta = i\Delta - ig\bar{x} + \gamma$ and $\Phi = \frac{d^2}{dt^2} + \gamma_m\frac{d}{dt} + \omega_m^2$. In what follows, we ignore the higher-order perturbation terms and use the following ansatz:

$$\begin{aligned}
\delta a_{\rm cw} &= \delta a_{\rm cw}^- e^{-i\xi t} + \delta a_{\rm cw}^+ e^{i\xi t}, \\
\delta a_{\rm ccw} &= \delta a_{\rm ccw}^- e^{-i\xi t} + \delta a_{\rm ccw}^+ e^{i\xi t}, \\
\delta x &= \delta x_1 e^{-i\xi t} + \delta x_1^* e^{i\xi t},
\end{aligned} \tag{8}$$

where $\delta a_{\rm cw}^-$ ($\delta a_{\rm cw}^+$) and $\delta a_{\rm ccw}^-$ ($\delta a_{\rm ccw}^+$) are the first-order upper (lower) sidebands of CW and CCW modes, respectively. Here, δx_1 is the first-order sideband of mechanical mode. Substitution of Eqs. (8) into Eqs. (7) leads to

$$\begin{aligned}
&f_1\delta a_{\rm cw}^- + iJ_1\delta a_{\rm cw}^- - ig\bar{a}_{\rm cw}\delta x_1 = \sqrt{\gamma_{\rm ex}}E_p, \\
&f_2\delta a_{\rm cw}^+ + iJ_1\delta a_{\rm cw}^+ - ig\bar{a}_{\rm cw}\delta x_1^* = 0, \\
&f_1\delta a_{\rm ccw}^- + iJ_2\delta a_{\rm cw}^- - ig\bar{a}_{\rm ccw}\delta x_1 = 0, \\
&f_2\delta a_{\rm ccw}^+ + iJ_2\delta a_{\rm cw}^+ - ig\bar{a}_{\rm ccw}\delta x_1^* = 0, \\
&\Xi_1\delta x_1 - \hbar g\sum_{i={\rm cw,ccw}}(\bar{a}_i^*\delta a_i^- + \bar{a}_i\delta a_i^{+*}) = 0,
\end{aligned} \tag{9}$$

where $f_{1,2} = \Theta \mp i\xi$ and $\Xi_1 = m_{\rm eff}(-\xi^2 - i\xi\gamma_m + \omega_m^2)$. By solving Eqs. (9), we obtain

$$\delta a_{\rm cw1}^- = \sqrt{\gamma_{\rm ex}}E_p\frac{i\hbar g^2|\bar{a}_{\rm ccw}|^2 f_3 - f_1 f_3\Xi_1 + \hbar g^2 f_1 f_5}{-f_1 f_3 f_4\Xi_1 + \hbar g^2 f}, \tag{10}$$

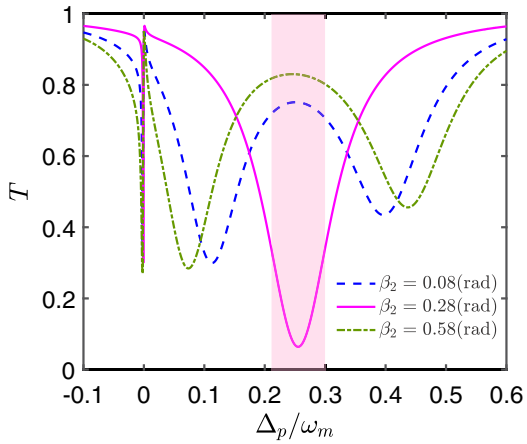

FIG. 3. The transmission rate T as a function of the probe detuning Δ_p and the relative angle β_2. The parameters used are $P_l = 1$ mW, $\Delta_a/\omega_m = 1$, and $\beta_1 = 0.57$; other parameters are the same as in Fig. 2.

where

$$
\begin{aligned}
f_3 &= f_2^2 + J_1^* J_2^*, \\
f_4 &= f_1 + J_1 J_2 / f_1, \\
f_5 &= J_1^* \bar{a}_{\mathrm{ccw}}^* \bar{a}_{\mathrm{cw}} + J_2^* \bar{a}_{\mathrm{cw}}^* \bar{a}_{\mathrm{ccw}} - i f_2 (|\bar{a}_{\mathrm{cw}}|^2 + |\bar{a}_{\mathrm{ccw}}|^2), \\
f_6 &= J_2 \bar{a}_{\mathrm{ccw}}^* \bar{a}_{\mathrm{cw}} + J_1 \bar{a}_{\mathrm{cw}}^* \bar{a}_{\mathrm{cw}} + i f_1 (|\bar{a}_{\mathrm{cw}}|^2 + |\bar{a}_{\mathrm{ccw}}|^2), \\
f &= f_3 f_6 + f_1 f_4 f_5. \qquad (11)
\end{aligned}
$$

By using the input-output relation, we obtain the transmission rate of the probe field

$$
T = |t_p|^2 = \left| 1 - \frac{\sqrt{\gamma_{\mathrm{ex}}}}{E_p} \delta a_{\mathrm{cw}}^- \right|^2 . \qquad (12)
$$

In the following, we discuss in detail the impact of the nanoparticles on the transmission rate and group delay in the vicinities of EPs with experimentally feasible parameters.

III. RESULTS AND DISCUSSION

The generation of OMIT highly depends on the detuning Δ_p and can be influenced by the relative positions of nanoparticles β_1 and β_2, where $\Delta_p = \omega_p - \omega_l$ is the probe detuning between the probe and cavity fields. Therefore the influence of both (i.e., Δ_p and $\beta_{1,2}$) on OMIT is mainly discussed in the following. First, we investigate the dependence of the transmission rate on the detuning Δ_p while keeping the relative position of nanoparticles fixed, as shown in Fig. 3. The figure shows the emergence of a Fano-like spectrum around the resonance due to the interference between the probe and the scattered control field. When Δ_p increases, a transparency window emerges at $\Delta_p/\omega_m \approx 0.255$ for β_2 values of 0.08 or 0.58. However, when steering the position of the third nanoparticle to bring the system close to the EPs (e.g., $\beta_2 = 0.28$), the transmission rate decreases steadily until it drops below 0.07 with increasing Δ_p, indicating that the system experiences strong absorption of the probe light in the vicinities of EPs, as indicated by the pink curve in Fig. 3. This intriguing result means that by adjusting the relative positions of three nanoparticles to bring the system close to EPs using a nanopositioner, one can effectively control the transmission rate of the probe light and achieve optical switching at $\Delta_p/\omega_m \approx 0.255$. Furthermore, using the property of the transmission rate in the vicinities of EPs enables us to infer the presence and approximate positions of the nanoparticle, facilitating particle detection. Our findings may provide theoretical guidance for optically sensitive detection.

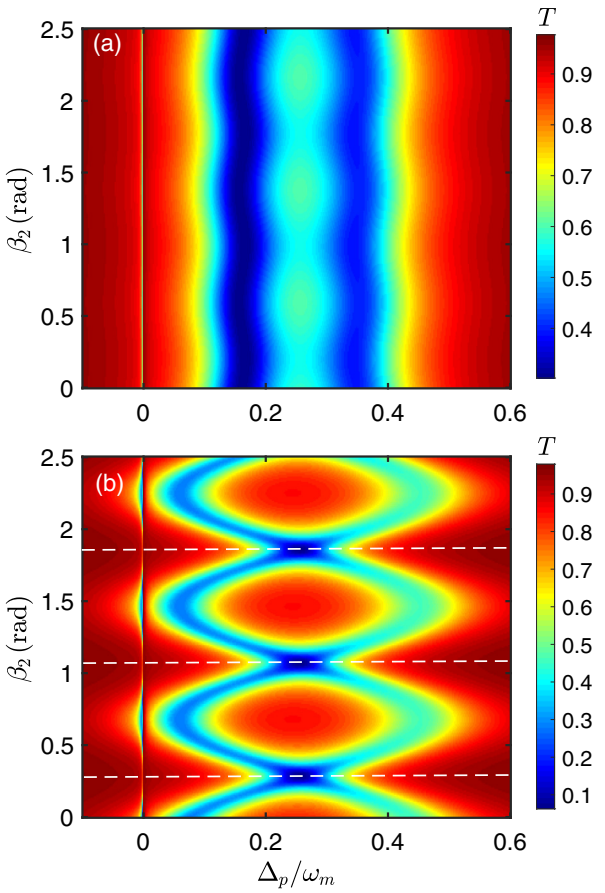

FIG. 4. Transmission rate T as a function of the probe detuning Δ_p and the relative angle β_2. The parameters are the same as in Fig. 3 except for (a) $\beta_1 = 0.4$ and (b) $\beta_1 = 0.57$.

To fully investigate the impact of the detuning Δ_p and the relative positions of the third nanoparticle β_2 on the transmission rate, in Fig. 4, we present the phase diagram in terms of the Δ_p and β_2. In Fig. 4(a), we fixed the relative positions of two nanoparticles at $\beta_1 = 0.4$, where the system exhibits a large eigenfrequency splitting, indicating that it is far from the EPs (not shown). Due to the minor influence of β_2 on the complex frequency splitting, the transmittance rate shows insensitivity to change in β_2. Hence the transmission rate has a minor change, regardless of the chosen value of β_2, when the detuning Δ_p is fixed. As a result, manipulating the position of the third nanoparticle cannot impact the transmittance rate of the probe light, making it impossible to accurately detect the third nanoparticle when β_1 is not within an appropriate range. Furthermore, the transmittance rate demonstrates limited sensitivity to the detuning of Δ_p, which is inadequate for detecting the third nanoparticle. However, when β_1 is in a

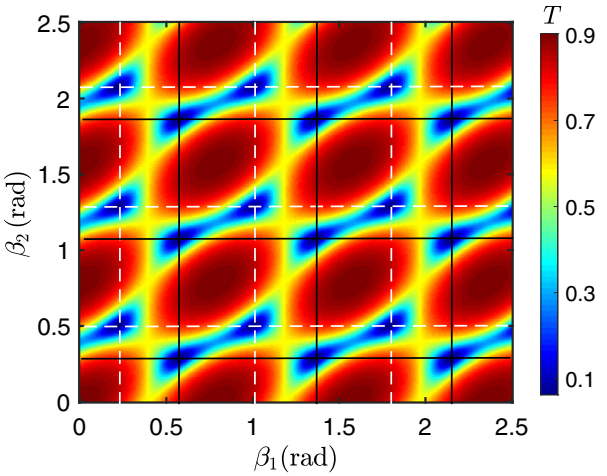

FIG. 5. Transmission rate T as a function of the relative angles β_1 and β_2. The parameters are the same as in Fig. 3 except for $\Delta_p/\omega_m = 0.255$.

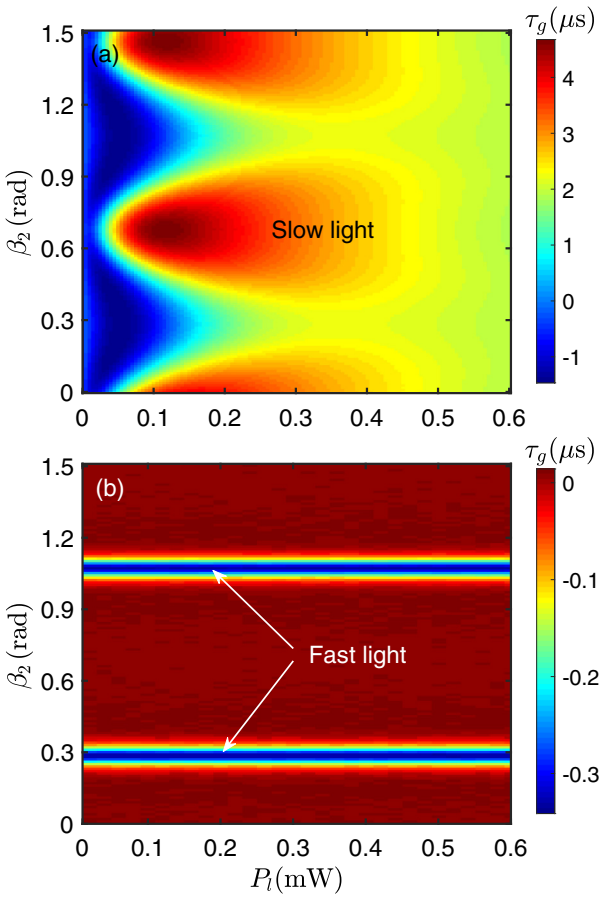

FIG. 6. Group delay τ_g (in units of microseconds) as a function of the pump power P_l and the relative angle β_2 when fixing the the relative angle $\beta_1 = 0.57$. (a) $\Delta_p/\omega_m = 0$ and (b) $\Delta_p/\omega_m = 0.255$; the other parameters are the same as in Fig. 2.

relatively appropriate position, β_2 can be calculated through spectral analysis, thus detecting the position. For example, when $\beta_1 = 0.57$, the system can experience EPs with increasing angle β_2 [see Fig. 2(b)], which leads to the transmittance rate reaching the minimum value in the vicinities of EPs, as shown in Fig. 4(b). This clearly shows that the transmittance rate changes periodically and coincides with the periodic appearance of EPs with the regulation of the angles β_1 and β_2, as indicated by the white dashed lines in Fig. 4(b). This result further demonstrates the role of EPs in the transmittance rate. Moreover, Fig. 4(b) also reveals the impact of the detuning Δ_p on the transmittance rate, and one can see that the minimum value is reached only when $\Delta_p/\omega_m = 0.255$, which coincides with the result of Fig. 3. The above results further confirm the advantage of tuning the system to the EPs for nanoparticle detection.

Toward a more comprehensive understanding of the impact of the relative position of the three nanoparticles on the transmission rate, we present a phase diagram in Fig. 5, which effectively elucidates the intricate relationship between the transmission rate and the angles β_1 and β_2. Note that the intersectionswhere the white dashed lines meet and the intersections where the black solid lines meet signify the system being in the EPs state. Figure 5 clearly shows the emergence of EP periodicity when tuning the angles β_1 and β_2, which is consistent with the results of Fig. 2. Moreover, it is evident that by fixing β_1 near the EPs, such as $\beta_1 \approx 0.215, 0.57, 1.01, 1.355, 1.79, 2.14$, rotating the third nanoparticle (i.e., changing the angle β_2) will significantly affect the change in the transmission rate. For example, tuning the angle β_2 towards EPs causes a significant reduction in dropping below 0.1 and potentially reaching 0, i.e., the probe light is significantly absorbed or even completely absorbed. Conversely, when the system is away from EPs, the transmission rate exceeds 0.9, indicating a state of probe light transparency. These findings not only validate the results illustrated in Fig. 3 but also offer a more comprehensive elucidation of the influence of the relative positions of the three nanoparticles on the transmission rate. Based on the above results, we can ascertain the existence and approximate location of the third nanoparticle by manipulating the positions of the two known nanoparticles, thereby achieving nanoparticle detection.

With the generation of OMIT, the slow-light effect can also occur, which is related to the anomalous dispersion of light and can be described by the optical group delay

$$\tau_g = \frac{d\arg(t_p)}{d\Delta_p}, \tag{13}$$

where $\arg(t_p)$ represents the phase of t_p. This implies that a more rapid phase dispersion leads to larger group delays, and vice versa. The relationship between group velocity τ_g and group delay v_g is $\tau_g = L(1/v_g - 1/c)$, where L is the distance that light travels and c is the speed of light in a vacuum. This clearly shows that $\tau_g > 0$ ($v_g < c$) and $\tau_g < 0$ ($v_g > c$) correspond to the slow light and fast light, respectively. Figure 6(a) shows that the group delay τ_g changes significantly when tuning the relative angle of nanoparticles β_2 and the pump power P_l. For $\Delta_p = 0$, it is possible to adjust the group delay to have either a positive or a negative value, indicating that by controlling the angle of the nanoparticles, one has the ability to not only cause a shift in the optical mode but also significantly alter the dispersion of the system. In order

to show the impact of the detuning Δ_p on group delay, in Fig. 6(b) we demonstrate how the group delay varies with the angle β_2 and P_l when $\Delta_p/\omega_m = 0.255$. The figure clearly shows that when steering the angle of β_2 to the vicinity of EPs, fast light emerges. However, slow light occurs when steering the angle β_2 away from the EPs. This means that the transition between slow and fast light can be achieved by manipulating the relative positions of the nanoparticles when $\Delta_p/\omega_m = 0.255$. Furthermore, one can use this property to detect the existence of nanoparticles.

IV. CONCLUSIONS

In conclusion, we have theoretically investigated OMIT in a WGM microresonator coupled with three nanoparticles. We showed that the transmission rate becomes more sensitive in the vicinities of EPs when the third nanoparticle is present. Additionally, by adjusting the relative position of the nanoparticles, we can switch the probe light between slow and fast light, depending on whether the system is near or far from the EPs. Our work may not only offer an alternative method to control the propagation of light but also enable the detection of a third particle by observing alterations in the output light spectrum, thus achieving particle detection. Our research may have a potential application for optical signal processing and communication.

ACKNOWLEDGMENTS

We acknowledge National Natural Science Foundation of China (Grants No. 12304395, No. 12005078, No. 12004202, and No. 12105210), National Key Research and Development Program of China (Grant No. 2021YFA1400700), Jianghan University Natural Science General Project (Grant No. 2021yb028), Luoyang Institute of Science and Technology Natural Science General Project (Grant No. 21010777), Chunhui Project Foundation of the Education Department of China (Grant No. HZKY20220337), and Natural Science Foundation of Hubei Province (Grant No. 2023AFB891).

[1] M. Aspelmeyer, T. J. Kippenberg, and F. Marquardt, Cavity optomechanics, Rev. Mod. Phys. **86**, 1391 (2014).
[2] P. Rabl, Photon blockade effect in optomechanical systems, Phys. Rev. Lett. **107**, 063601 (2011).
[3] A. Nunnenkamp, K. Børkje, and S. M. Girvin, Single-photon optomechanics, Phys. Rev. Lett. **107**, 063602 (2011).
[4] R. Yalla, F. LeKien, M. Morinaga, and K. Hakuta, Efficient channeling of fluorescence photons from single quantum dots into guided modes of optical nanofiber, Phys. Rev. Lett. **109**, 063602 (2012).
[5] J. Qian, A. A. Clerk, K. Hammerer, and F. Marquardt, Quantum signatures of the optomechanical instability, Phys. Rev. Lett. **109**, 253601 (2012).
[6] Y.-Y. Zhou, J. Yu, Z.-H. Yan, X.-J. Jia, J. Zhang, C.-D. Xie, and K.-C. Peng, Quantum secret sharing among four players using multipartite bound entanglement of an optical field, Phys. Rev. Lett. **121**, 150502 (2018).
[7] G.-L. Zhu, X.-Y. Lü, L.-L. Wan, T.-S. Yin, Q. Bin, and Y. Wu, Controllable nonlinearity in a dual-coupling optomechanical system under a weak-coupling regime, Phys. Rev. A **97**, 033830 (2018).
[8] C.-S. Hu, L.-T. Shen, Z.-B. Yang, H. Wu, Y. Li, and S.-B. Zheng, Manifestation of classical nonlinear dynamics in optomechanical entanglement with a parametric amplifier, Phys. Rev. A **100**, 043824 (2019).
[9] Q. Bin, X.-Y. Lü, F. P. Laussy, F. Nori, and Y. Wu, N-phonon bundle emission via the Stokes process, Phys. Rev. Lett. **124**, 053601 (2020).
[10] Y.-H. Liu, X.-L. Yin, J.-F. Huang, and J.-Q. Liao, Accelerated ground-state cooling of an optomechanical resonator via shortcuts to adiabaticity, Phys. Rev. A **105**, 023504 (2022).
[11] D.-G. Lai, J.-Q. Liao, A. Miranowicz, and F. Nori, Noise-tolerant optomechanical entanglement via synthetic magnetism, Phys. Rev. Lett. **129**, 063602 (2022).
[12] Y. Zhou, C.-S. Hu, D.-Y Lü, X.-K. Li, H.-M. Huang, Y.-C. Xiong, and X.-Y. Lü, Synergistic enhancement of spin-phonon interaction in a hybrid system, Photonics Res. **10**, 1640 (2022).
[13] C. Fabre, M. Pinard, S. Bourzeix, A. Heidmann, E. Giacobino, and S. Reynaud, Quantum-noise reduction using a cavity with a movable mirror, Phys. Rev. A **49**, 1337 (1994).
[14] R. Ghobadi, A. R. Bahrampour, and C. Simon, Quantum optomechanics in the bistable regime, Phys. Rev. A **84**, 033846 (2011).
[15] S. Aldana, C. Bruder, and A. Nunnenkamp, Equivalence between an optomechanical system and a Kerr medium, Phys. Rev. A **88**, 043826 (2013).
[16] T. J. Kippenberg, H. Rokhsari, T. Carmon, A. Scherer, and K. J. Vahala, Analysis of radiation-pressure induced mechanical oscillation of an optical microcavity, Phys. Rev. Lett. **95**, 033901 (2005).
[17] F. Marquardt, J. G. E. Harris, and S. M. Girvin, Dynamical multistability induced by radiation pressure in high-finesse micromechanical optical cavities, Phys. Rev. Lett. **96**, 103901 (2006).
[18] C. Metzger, M. Ludwig, C. Neuenhahn, A. Ortlieb, I. Favero, K. Karrai, and F. Marquardt, Self-induced oscillations in an optomechanical system driven by bolometric backaction, Phys. Rev. Lett. **101**, 133903 (2008).
[19] S. Zaitsev, A. K. Pandey, O. Shtempluck, and E. Buks, Forced and self-excited oscillations of an optomechanical cavity, Phys. Rev. E **84**, 046605 (2011).
[20] G. Heinrich, M. Ludwig, J. Qian, B. Kubala, and F. Marquardt, Collective dynamics in optomechanical arrays, Phys. Rev. Lett. **107**, 043603 (2011).
[21] C. A. Holmes, C. P. Meaney, and G. J. Milburn, Synchronization of many nanomechanical resonators coupled via a common cavity field, Phys. Rev. E **85**, 066203 (2012).
[22] M. Zhang, G. S. Wiederhecker, S. Manipatruni, A. Barnard, P. McEuen, and M. Lipson, Synchronization of micromechanical oscillators using light, Phys. Rev. Lett. **109**, 233906 (2012).

[23] K. Børkje, A. Nunnenkamp, J. D. Teufel, and S. M. Girvin, Signatures of nonlinear cavity optomechanics in the weak coupling regime, Phys. Rev. Lett. **111**, 053603 (2013).

[24] A. G. Krause, J. T. Hill, M. Ludwig, A. H. Safavi-Naeini, J. Chan, F. Marquardt, and O. Painter, Nonlinear radiation pressure dynamics in an optomechanical crystal, Phys. Rev. Lett. **115**, 233601 (2015).

[25] D. Navarro-Urrios, N. E. Capuj, M. F. Colombano, P. D. Garcia, M. Sledzinska, F. Alzina, A. Griol, A. Martinez, and C. M. Sotomayor-Torres, Nonlinear dynamics and chaos in an optomechanical beam, Nat. Commun. **8**, 14965 (2017).

[26] Y.-L. Liu, C. Wang, J. Zhang, and Y.-X. Liu, Cavity optomechanics: Manipulating photons and phonons towards the single-photon strong coupling, Chin. Phys. B **27**, 024204 (2018).

[27] C.-L. Zhu, Y.-L. Liu, L. Yang, Y.-X. Liu, and J. Zhang, Synchronization in $\mathcal{PT}$-symmetric optomechanical resonators, Photonics Res. **9**, 2152 (2021).

[28] O. Arcizet, P.-F. Cohadon, T. Briant, M. Pinard, A. Heidmann, J.-M. Mackowski, C. Michel, L. Pinard, O. Français, and L. Rousseau, High-sensitivity optical monitoring of a micromechanical resonator with a quantum-limited optomechanical sensor, Phys. Rev. Lett. **97**, 133601 (2006).

[29] I. S. Grudinin, H. Lee, O. Painter, and K. J. Vahala, Phonon laser action in a tunable two-level system, Phys. Rev. Lett. **104**, 083901 (2010).

[30] J. Chan, T. P. M. Alegre, A. H. Safavi-Naeini, J. T. Hill, A. Krause, S. Gröblacher, M. Aspelmeyer, and O. Painter, Laser cooling of a nanomechanical oscillator into its quantum ground state, Nature (London) **478**, 89 (2011).

[31] J. D. Teufel, T. Donner, D. Li, J. W. Harlow, M. S. Allman, K. Cicak, A. J. Sirois, J. D. Whittaker, K. W. Lehnert, and R. W. Simmonds, Sideband cooling of micromechanical motion to the quantum ground state, Nature (London) **475**, 359 (2011).

[32] E. Gavartin, P. Verlot, and T. J. Kippenberg, A hybrid on-chip optomechanical transducer for ultrasensitive force measurements, Nat. Nanotechnol. **7**, 509 (2012).

[33] T. Bagci, A. Simonsen, S. Schmid, L. G. Villanueva, E. Zeuthen, J. Appel, J. M. Taylor, A. Sørensen, K. Usami, A. Schliesser, and E. S. Polzik, Optical detection of radio waves through a nanomechanical transducer, Nature (London) **507**, 81 (2014).

[34] E. E. Wollman, C. U. Lei, A. J. Weinstein, J. Suh, A. Kronwald, F. Marquardt, A. A. Clerk, and K. C. Schwab, Quantum squeezing of motion in a mechanical resonator, Science **349**, 952 (2015).

[35] F. Lecocq, J. B. Clark, R. W. Simmonds, J. Aumentado, and J. D. Teufel, Mechanically mediated microwave frequency conversion in the quantum regime, Phys. Rev. Lett. **116**, 043601 (2016).

[36] C. U. Lei, A. J. Weinstein, J. Suh, E. E. Wollman, A. Kronwald, F. Marquardt, A. A. Clerk, and K. C. Schwab, Quantum nondemolition measurement of a quantum squeezed state beyond the 3 dB limit, Phys. Rev. Lett. **117**, 100801 (2016).

[37] G. S. Agarwal and S. Huang, Electromagnetically induced transparency in mechanical effects of light, Phys. Rev. A **81**, 041803(R) (2010).

[38] S. Weis, R. Rivière, S. Deléglise, E. Gavartin, O. Arcizet, A. Schliesser, and T. J. Kippenberg, Optomechanically induced transparency, Science **330**, 1520 (2010).

[39] A. H. Safavi-Naeini, T. P. M. Alegre, J. Chan, M. Eichenfield, M. Winger, Q. Lin, J. T. Hill, D. E. Chang, and O. Painter, Electromagnetically induced transparency and slow light with optomechanics, Nature (London) **472**, 69 (2011).

[40] H. Xiong, L.-G. Si, A.-S. Zheng, X. Yang, and Y. Wu, Higher-order sidebands in optomechanically induced transparency, Phys. Rev. A **86**, 013815 (2012).

[41] Y. F. Jiao, T. X. Lu, and H. Jing, Optomechanical second-order sidebands and group delays in a Kerr resonator, Phys. Rev. A **97**, 013843 (2018).

[42] H. Wang, X. Gu, Y.-x. Liu, A. Miranowicz, and F. Nori, Optomechanical analog of two-color electromagnetically induced transparency: Photon transmission through an optomechanical device with a two-level system, Phys. Rev. A **90**, 023817 (2014).

[43] P.-C. Ma, J.-Q. Zhang, Y. Xiao, M. Feng, and Z.-M. Zhang, Tunable double optomechanically induced transparency in an optomechanical system, Phys. Rev. A **90**, 043825 (2014).

[44] S. Huang, Double electromagnetically induced transparency and narrowing of probe absorption in a ring cavity with nanomechanical mirrors, J. Phys. B: At., Mol. Opt. Phys. **47**, 055504 (2014).

[45] B. P. Hou, L. F. Wei, and S. J. Wang, Optomechanically induced transparency and absorption in hybridized optomechanical systems, Phys. Rev. A **92**, 033829 (2015).

[46] C.-H. Dong, Z. Shen, C.-L. Zou, Y.-L. Zhang, W. Fu, and G.-C. Guo, Brillouin-scattering-induced transparency and nonreciprocal light storage, Nat. Commun. **6**, 6193 (2015).

[47] M. J. Akram, M. M. Khan, and F. Saif, Tunable fast and slow light in a hybrid optomechanical system, Phys. Rev. A **92**, 023846 (2015).

[48] C. Jiang, Y. Cui, X. Bian, F. Zuo, H. Yu, and G. Chen, Phase-dependent multiple optomechanically induced absorption in multimode optomechanical systems with mechanical driving, Phys. Rev. A **94**, 023837 (2016).

[49] Z. Shen, C.-H. Dong, Y. Chen, Y.-F. Xiao, F.-W. Sun, and G.-C. Guo, Compensation of the Kerr effect for transient optomechanically induced transparency in a silica microsphere, Opt. Lett. **41**, 1249 (2016).

[50] X. Y. Zhang, Y. H. Zhou, Y. Q. Guo, and X. X. Yi, Optomechanically induced transparency in optomechanics with both linear and quadratic coupling, Phys. Rev. A **98**, 053802 (2018).

[51] T.-X. Lu, Y.-F. Jiao, H.-L. Zhang, F. Saif, and H. Jing, Selective and switchable optical amplification with mechanical driven oscillators, Phys. Rev. A **100**, 013813 (2019).

[52] Z. Shen, Y.-L. Zhang, Y. Chen, C.-L. Zou, Y.-F. Xiao, X.-B. Zou, F.-W. Sun, G.-C. Guo, and C.-H. Dong, Experimental realization of optomechanically induced non-reciprocity, Nat. Photonics **10**, 657 (2016).

[53] H. Lü, Y. Jiang, Y.-Z. Wang, and H. Jing, Optomechanically induced transparency in a spinning resonator, Photonics Res. **5**, 367 (2017).

[54] C. M. Bender and S. Boettcher, Real spectra in non-Hermitian Hamiltonians having $\mathcal{PT}$ symmetry, Phys. Rev. Lett. **80**, 5243 (1998).

[55] C. M. Bender, Making sense of non-Hermitian Hamiltonians, Rep. Prog. Phys. **70**, 947 (2007).

[56] C. E. Rüter, K. G. Makris, R. El-Ganainy, D. N. Christodoulides, M. Segev, and D. Kip, Observation of parity-time symmetry in optics, Nat. Phys. **6**, 192 (2010).

[57] A. A. Zyablovsky, A. P. Vinogradov, A. A. Pukhov, A. V. Dorofeenko, and A. A. Lisyansky, PT-symmetry in optics, Phys. Usp. **57**, 1063 (2014).

[58] B. Peng, Ş. K. Özdemir, F. Lei, F. Monifi, M. Gianfreda, G. L. Long, S. Fan, F. Nori, C. M. Bender, and L. Yang, Parity-time-symmetric whispering-gallery microcavities, Nat. Phys. **10**, 394 (2014).

[59] V. V. Konotop, J. Yang, and D. A. Zezyulin, Nonlinear waves in $\mathcal{PT}$-symmetric systems, Rev. Mod. Phys. **88**, 035002 (2016).

[60] L. Feng, R. El-Ganainy, and L. Ge, Non-Hermitian photonics based on parity-time symmetry, Nat. Photonics **11**, 752 (2017).

[61] S. Longhi, Parity-time symmetry meets photonics: A new twist in non-Hermitian optics, Europhys. Lett. **120**, 64001 (2017).

[62] L. Feng, Z. J. Wong, R.-M. Ma, Y. Wang, and X. Zhang, Single-mode laser by parity-time symmetry breaking, Science **346**, 972 (2014).

[63] H. Hodaei, M.-A. Miri, M. Heinrich, D. N. Christodoulides, and M. Khajavikhan, Parity-time symmetric microring lasers, Science **346**, 975 (2014).

[64] H. Jing, Ş. K. Özdemir, X. Y. Lü, J. Zhang, L. Yang, and F. Nori, $\mathcal{PT}$-symmetric phonon laser, Phys. Rev. Lett. **113**, 053604 (2014).

[65] X. Y. Lü, H. Jing, J. Y. Ma, and Y. Wu, $\mathcal{PT}$-symmetry-breaking chaos in optomechanics, Phys. Rev. Lett. **114**, 253601 (2015).

[66] J. Wiersig, Enhancing the sensitivity of frequency and energy splitting detection by using exceptional points: application to microcavity sensors for single-particle detection, Phys. Rev. Lett. **112**, 203901 (2014).

[67] J. Wiersig, Sensors operating at exceptional points: General theory, Phys. Rev. A **93**, 033809 (2016).

[68] W. Chen, Ş. K. Özdemir, G. Zhao, J. Wiersig, and L. Yang, Exceptional points enhance sensing in an optical microcavity, Nature (London) **548**, 192 (2017).

[69] M. P. Hokmabadi, A. Schumer, D. N. Christodoulides, and M. Khajavikhan, Non-Hermitian ring laser gyroscopes with enhanced Sagnac sensitivity, Nature (London) **576**, 70 (2019).

[70] L. Chang, X. S. Jiang, S. Y. Hua, C. Yang, J. M. Wen, L. A Jiang, G. Y. Li, G. Z. Wang, and M. Xiao, Parity-time symmetry and variable optical isolation in active-passive-coupled microresonators, Nat. Photonics **8**, 524 (2014).

[71] B. Peng, Ş. K. Özdemir, M. Liertzer, W. Chen, J. Kramer, H. Yılmaz, J. Wiersig, S. Rotter, and L. Yang, Chiral modes and directional lasing at exceptional points, Proc. Natl. Acad. Sci. USA **113**, 6845 (2016).

[72] H. Lü, C. Wang, and H. Jing, Optomechanically induced transparency at exceptional points, Phys. Rev. Appl. **10**, 014006 (2018).

[73] J. Zhu, Ş. K. Özdemir, L. He, and L. Yang, Controlled manipulation of mode splitting in an optical microcavity by two Rayleigh scatterers, Opt. Express **18**, 23535 (2010).